Determining Salient Control Decisions of the Actuated Spring Loaded Inverted Pendulum Traversing Slippery Terrain Using a Sliding Mass Model

Samuel Pfrommer

January 19, 2017

Abstract

Legged robot running has long been modeled using a Spring Loaded Inverted Pendulum (SLIP). While the SLIP model has been found to accurately match important dynamic running characteristics such as ground reaction force profiles, it is also highly nonlinear and has no closed-form solution. This study proposes an analytically solvable sliding mass model for predicting energy-optimal key control decisions for a SLIP on low-friction terrain. To evaluate sliding mass model predictions, a series of test scenarios are generated. Each scenario consists of a randomly sized slippery patch with the SLIP positioned randomly over the patch, analogous to a legged running robot stepping on an unforeseen ice patch. Two possibilities are then considered for traversing the patch: stepping back onto firm ground first and then launching over the patch (three stance phases) or stepping directly from the patch to the goal (two stance phases). In order to determine the true energy-optimal solution, both situations are transcribed as numerical trajectory optimization problems using direct collocation. The optimal step sequence from the optimizer is then compared with the output of the simplified sliding mass model, which was found to determine the best sequence with 88% accuracy. These results suggest that sliding mass models can be used to traverse unexpected terrain features in real time, whereas true trajectory optimization often takes prohibitively long to converge. Embracing similar control techniques could lead to the use of legged robots in previously inaccessible terrain, such as a disaster scene or complex natural environment. Qualitative analysis of repeated solution patterns also suggests that there exist several distinctive control strategies that are applied for various classes of initial states, teasing possible future controller development based on templated motion patterns.

1 Introduction

Bipedal robots are complex machines, usually involving dozens of degrees of freedom. Planning dynamic motions with so many free variables is often computationally infeasible; therefore, multiple simplified templates have been developed to describe the fundamental dynamics of more complicated robots. Foremost among these is the Spring Loaded Inverted Pendulum (SLIP) model, which approximates the mass of the robot to a point at the hip and each leg to a spring.

The details of the SLIP model vary from study to study. Mark Raibert's groundbreaking hoppers in the 1980's employed both hip torque and radial actuation in empirical control procedures (Raibert et al., 1986)—it was not until decades later, however, that SLIP theory developed to formalize the field. Even the passive, unactuated SLIP equations are analytically unsolvable, and various stance-phase approximations have had to be developed to predict passive SLIP center-of-mass motion (Saranli et al., 2010). Later analyses such as (Piovan and Byl, 2012) considered the effect of radial actuation along the leg on symmetry enforcement within stance phases. In (Larson and Seipel, 2012), the stability of radial actuation was analyzed, this time including a damper in series with the spring. Other studies have examined running control using a Hybrid Zero Dynamics framework, incorporating both hip torque and radial forcing (Poulakakis and Grizzle, 2007)

Most SLIP studies have focused explicitly on situations where ground slippage is not an issue—in other words, infinite friction is assumed. Preliminary research on slippage was again conducted at the MIT Leg Lab, where mathematically non-rigorous reflexes helped SLIP hoppers recover on low-friction terrain (Boone and Hodgins, 1997). Rigorous mathematical analyses began with (Gamus and Or, 2013), where rimless wheel and compass biped walker gaits were analyzed while allowing for stick-slip transitions. In Or and Moravia (2016), the full SLIP model was considered, including hip torque actuation, damping, and an additional toe mass.

Conventional research on SLIP hoppers has generally focused on limit cycle planning—examining how the SLIP converges to stable gaits over many steps. One popular tool for analyzing SLIP trajectories over long distances has been numerical trajectory optimization, which essentially uses a form of gradient descent to numerically search for energy-optimal trajectories while allowing for certain constraints (e.g., the trajectory must have a certain time duration). In (Srinivasan and Ruina, 2006), numerical trajectory optimization was used to discover that different gait patterns—inverted pendulum walking, pendular running, impulsive running—are energetically efficient at different target speeds. Later research analyzed how optimizing for various artificial tasks resulted in different asymptotically-stable limit cycles (Hubicki et al., 2015).

This study analyzes short-term traversal patterns for the SLIP hopper on hybrid low-and-high-friction terrain. To the author's knowledge, it is the first time numerical trajectory optimization has been applied to SLIPs on slippery surfaces, although some studies have been performed on granular media (Hubicki et al., 2016). Using inspiration from (Hubicki et al., 2015), a one-dimensional sliding mass model is developed to approximate SLIP trajectories and predict energy-optimal step sequences for traversing the slippery patch.

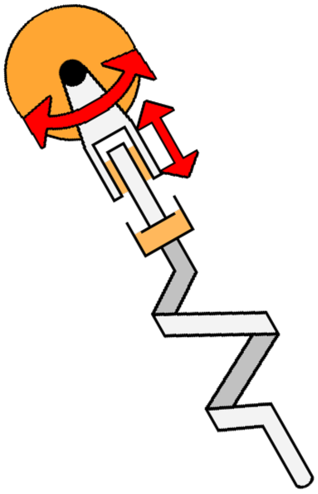

Figure 1: The Spring Loaded Inverted Pendulum (SLIP) model used in this experiment, with a spring and damper. The two red arrows represent actuation—one the hip torque, and the other the second derivative of the neutral spring length.

2 Methods

2.1 SLIP Model

The SLIP used in this experiment featured a damper, radial actuator (controls second derivative of neutral leg length, or $\ddot{r_a}$), and hip torque actuator (Figure 1). The parameters for the Spring Loaded Inverted Pendulum were as follows:

Parameters for the SLIP hopper were repeated from (Hubicki et al., 2015) and are proportional to human running parameters. The slip phase friction coefficient was chosen manually to roughly approximate contact between an ice patch and a rubbery foot.

Parameter	Value
Max Length	1m
Min Length	0.5m
Hip Mass	1kg
Toe Mass	0.1kg
Spring coefficient	20N/m
Damping coefficient	0.5
Max hip torque	±1
Max $\ddot{r_a}$	±1
Gravity	$1m/s^2$
Slip friction coefficient	0.05

Table 1: A table describing various parameters for the SLIP hopper simulations.

2.2 SLIP Equations of Motions

We will now review the equations of motions for the SLIP. Let (x,y) be the hip position, x_{toe} be the toe horizontal position, k be the spring coefficient, c be the damping coefficient, r be the SLIP length, r_a be the actuated SLIP length (or neutral spring length), τ be the hip torque, m_{hip} and m_{toe} be the hip and toe masses, respectively, and g be the gravitational constant. r can then be written as:

$$r = \sqrt{(x - x_{toe})^2 + y^2} \tag{1}$$

Differentiating by the chain rule, we get the following equation for the time derivative of r:

$$\dot{r} = \frac{(x - x_{toe}) \cdot (\dot{x} - \dot{x_{toe}}) + y\dot{y}}{r} \tag{2}$$

The force exerted by the spring-damper combination can then be expressed as follows:

$$F_s = k(r_a - r) + c(\dot{r_a} - \dot{r}) \tag{3}$$

While the force exerted by the hip torque on the ground is simply:

$$F_t = \frac{\tau}{r} \tag{4}$$

Realizing that the cosine of the angle between the SLIP and the ground is equal to $\frac{x - x_{toe}}{r}$ and the sine is equal to $\frac{y}{r}$, it is possible to express the acceleration of the hip:

$$\ddot{x} = \frac{1}{m_{hip}} \cdot (F_s \frac{x - x_{toe}}{r} + F_t \frac{y}{r}) \tag{5}$$

$$\ddot{y} = \frac{1}{m_{hip}} \cdot (F_s \frac{y}{r} - F_t \frac{x - x_{toe}}{r} - m_{hip} \cdot g) \tag{6}$$

However, it is also necessary to know the acceleration of the toe on the ice. We first determine the ground reaction force as follows:

$$GRF = F_s \frac{y}{r} - F_t \frac{x - x_{toe}}{r} + m_{toe} g \tag{7}$$

The force of friction on the toe is then given as:

$$F_f = -\mu \cdot \tanh(50\dot{x_{toe}}) \cdot GRF \tag{8}$$

Where the $\tanh(50\dot{x_{toe}})$ serves as a smooth approximation of a sign function, whose discontinuities create convergence difficulties for the optimizer.

Finally, the acceleration of the toe can be expressed as follows:

$$\ddot{x_{toe}} = \begin{cases} 0 & \text{if stick phase} \\ \frac{1}{m_{toe}} \cdot (-F_s \frac{x - x_{toe}}{r} - F_t \frac{y}{r} + F_f) & \text{if slip phase} \end{cases} \tag{9}$$

This concludes the SLIP dynamics during stance phase. Flight phase dynamics initiate when the ground reaction force intersects zero and are governed by the canonical equations for ballistic trajectories.

2.3 Experimentation

217 experiments were performed. In each case, a random ice patch was generated with a width of between 0.8 and 1.8 meters. The SLIP x position was initialized to a random location over the ice patch, allowing for at least a 0.3 meter margin from each side. Since the robot was assumed to be running in the positive x direction upon unexpectedly encountering the ice patch, the initial hip x velocity was randomly distributed between 0m/s and 0.5m/s, and the initial hip y velocity was randomly distributed between 0m/s and -0.4m/s. The toe started off contacting the ice a random distance within 0.2 meters in front of

the hip. The initial y value was inferred from the toe x and hip x using the assumption that the leg is fully extended at the moment of touchdown. Additionally, at touchdown $r_a = r$ and $\dot{r_a} = 0$.

Two candidate step sequences were then considered: immediately stepping from the slippery surface to the ground on the right of the patch (two stance phases), or first stepping to the ground on the left and using the energy storage capabilities of the SLIP spring to launch over to the other side of the patch. Both cases were presented to the numerical trajectory optimizer (described in the next section), which found minimum-work trajectories for both step sequences. The optimal step sequence from the optimizer was then compared with the sliding mass model predictions.

2.4 Optimization Problem

To calculate the minimum work required for each step sequence, the trajectory optimization problem was transcribed into a function optimization problem using direct collocation. Each stance phase was discretized into ten evenly-spaced nodes, with an additional parameter for the time duration of each stance phase. Dynamics between nodes were enforced using trapezoidal quadrature. To link the end of one stance phase with the beginning of the next, a flight time parameter was included. The end hip position of the ballistic trajectory was then constrained to equal the hip position at the start of the next phase. The two candidate step sequences were formulated as separate optimization problems. After transcription, the programming problem was solved using MATLAB's *fmincon* function and the Sequential Quadratic Programming algorithm.

To facilitate more reliable convergence, the optimization was performed in three steps. First, the optimizer was given a constant objective function—in other words, it was instructed to find any trajectory that satisfied the constraints. The output trajectory was then fed into an impulse-squared objective function, which is relatively fast and reliable to optimize. Finally, the output of the impulse objective was fed into a work objective function. This method converged reliably from random initial guesses when solutions existed, usually in under two minutes.

Parameter	Value
Nodes per phase	10
Min stance time	0.1
Max stance time	2
Min flight time	0
Max flight time	5
Max GRF	10N

Table 2: A table of parameters for the numerical trajectory optimizer.

The following parameters were used for the optimizer:

2.5 Objective Function

The impulse cost function is as follows:

$$C_{imp} = \sum_{n=1}^{N_{phase}} \sum_{i=1}^{N_{grid}} [(\ddot{r}_{an,i} \cdot \Delta t_n)^2 + (\tau_{n,i} \cdot \Delta t_n)^2] \quad (10)$$

Where N_{phase} is the number of stance phases, N_{grid} is the number of discretization nodes per stance phase, and Δt_n is equal to the $\mathrm{n_{th}}$ stance phase time T_n divided by N_{grid}.

The work cost function is written as:

$$\sum_{n=1}^{N_{phase}} \left[\int_0^{T_n} |F_s \cdot \dot{r_a}| \, dt + \int_{\theta_{td}}^{\theta_{to}} |\tau d\theta| \right] \quad (11)$$

Since the absolute value function is inherently nonsmooth—creating optimizer convergence problems—a smooth approximation was employed for both cost functions, as described in (Hubicki et al., 2015).

$$|x| \approx \sqrt{x^2 + \epsilon^2} - \epsilon \quad (12)$$

Where ϵ is about 10^{-3}.

2.6 Sliding Mass Model

Here, a Sliding Mass Model is presented for predicting the energy-optimal step sequences given by the optimizer. The prediction occurs in two parts, first for the two-phase forwards sequence and then for the three-phase backwards sequence. Both methods are visualized back-to-back in Figure 2.

2.7 Forwards Sequence

Throughout these approximations, the SLIP is assumed to be close to vertical (ground angle = $\pi/2$). This allows the equations to be written without trigonometric expressions. We begin by considering the acceleration of the toe during the first stance phase:

$$a_{toe} = \frac{1}{m_{toe}} \cdot \frac{\tau_{max}}{r_{max}} - \mu g(m_{hip} + m_{toe}) \tag{13}$$

Where τ_{max} and r_{max} are the maximum hip torque and leg length, respectively. We now consider the maximum distance the toe can slide without leaving the slippery patch or losing ground contact. A maximum stance phase angle $\theta_{max} = 0.57$ is assumed. The distance covered by the toe behind the hip can be expressed as:

$$d_{back} = \min(\sin(\theta_{max}) \cdot r, x_0 - x_{sl}) \tag{14}$$

Where x_0 is the initial hip x position and x_{sl} is the x position of the left end of the slip patch.

The total toe travel distance can then be written as:

$$d_{toe} = x_{toe-0} - x_0 + d_{back} \tag{15}$$

Where x_{toe-0} is the initial toe position.

The work of the sliding phase can then be expressed:

$$W_{slide} = d_{toe} \cdot \frac{\tau_{max}}{r_{max}} \tag{16}$$

Which allows the time of the sliding phase to be written as follows, simplifying the toe to be relatively at rest initially (valid because of the large accelerations).

$$t_{slide} = \sqrt{\frac{2d_{toe}}{a_{toe}}} \tag{17}$$

The sliding mass displacement during the sliding phase can now be written as the following, again linearizing around the vertical:

$$x_{sf} = x_0 + \dot{x_0} \cdot t_{slide} + 0.5 \cdot \frac{\tau_{max}}{r_{max}} \cdot t_{slide}^2 \tag{18}$$

Before being able to calculate the flight penalty, we need to address the last "pull-up" phase, where the SLIP may have to lift itself to the final x target. This was approximated as a linear function of the initial distance to the end position and the initial velocity:

$$w_{pu} = \max(k_1 \cdot (x_{end} - x_0 - k_2) - k_3\dot{x_0}, 0) \tag{19}$$

Where x_{end} is the final x position that the sliding mass needs to reach (also the final x position of the SLIP in simulation) and $k_1 = 0.784$, $k_2 = 0.743$, $k_3 = 0.4$ are coefficients.

Approximating the SLIP as a simple inverted pendulum with the pivot at the foot, the x distance along the sliding mass axis can be expressed in terms of W_{pu} as follows:

$$\Delta X_{pu} = r_{max}\sqrt{1 - \left(1 - \frac{W_{pu}}{m_{hip} r_{max} g}\right)^2} \tag{20}$$

Finally, we can evaluate the penalty assigned to SLIP flight as follows (incorporating equations 18 and 20):

$$W_{flight} = (x_{end} - x_{sf} - \Delta X_{pu}) \cdot m_{hip} r_{max} k_{flight} \tag{21}$$

Where $k_{fleight} = 0.158$ is a weighting coefficient.

The cumulative work for the sequence, combining equations 16, 19, and 21 is expressed as:

$$W_{for} = W_{slide} + W_{flight} + W_{pu} \tag{22}$$

2.8 Backwards Sequence

To model the work for the backwards step sequence, the only additional assumption we make is the existence of a constant spring rebound segment on the sliding mass axis, $s_z = [0.117, 0.523]$. Equations 13, 16, and 17 remain the same, and equations 14 and 15 are modified slightly:

$$d_{front} = \min(\sin(\theta_{max}) \cdot r, x_{sr} - x_0) \tag{23}$$

$$d_{toe} = x_0 - x_{toe-0} + d_{front} \tag{24}$$

Where x_{sr} is the x position of the right end of the slip patch.

Equation 18 becomes:

$$x_{sf} = x_0 + \dot{x_0} \cdot t_{slide} - 0.5 \cdot \frac{\tau_{max}}{r_{max}} \cdot t_{slide}^2 \tag{25}$$

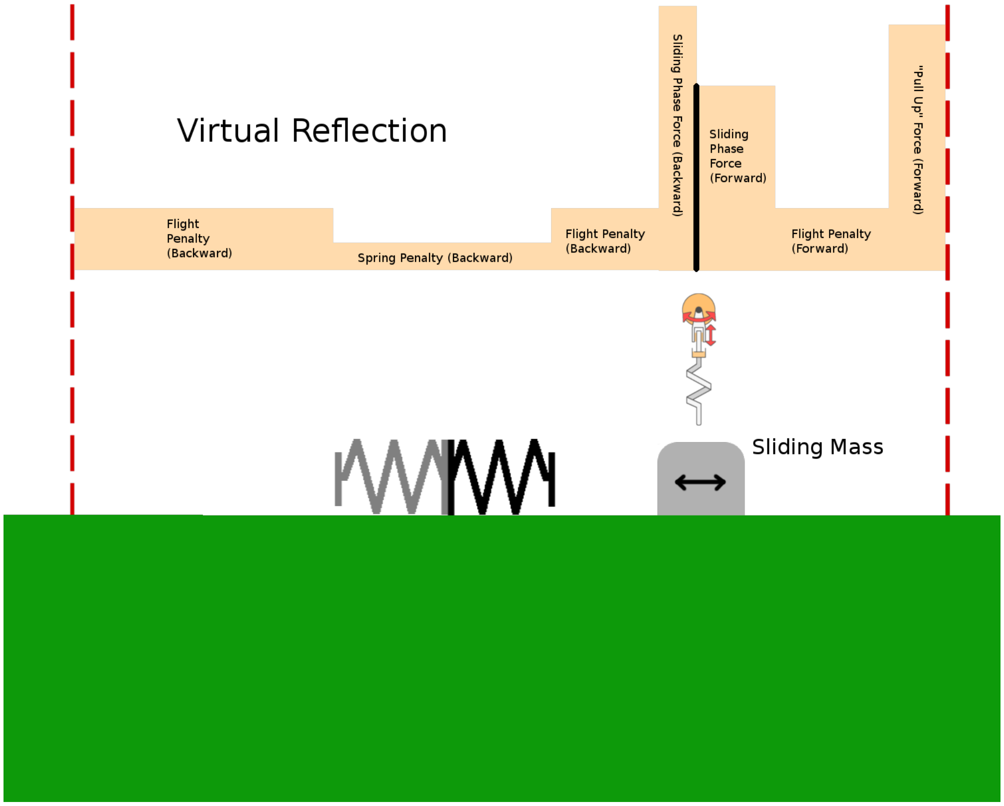
Virtual Reflection
Flight Penalty (Backward)
Spring Penalty (Backward)
Flight Penalty (Backward)
Sliding Phase Force (Backward)
Sliding Phase Force (Forward)
Flight Penalty (Forward)
"Pull Up" Force (Forward)
Sliding Mass

Figure 2: A visualization of the sliding mass model. The vertical black line above the SLIP and sliding mass divides the two possible step sequences. The light orange area represents work approximation for each of the key sections of the trajectory. Penalties are assigned to flight phases (loss of potential energy) and spring phases (damping losses), and work for sliding phases and stance phases are computed analytically using linearizations of SLIP dynamics.

Here, it is worthwhile to note an important corner case—when the sliding mass starts out within the spring zone, i.e. $x_0 < s_z(2)$. Then, $W_{su} = 0$ and correspondingly $x_{sf} = x_0$.

The spring zone work now becomes:

$$W_{sz} = 2 \cdot (s_z(2) - s_z(1)) \cdot m_{hip} g k_{sz} \tag{26}$$

Where $k_{sz} = 0.716$ is an arbitrary penalty coefficient taking into account spring damping and some measure of work against gravity.

The flight penalty for both corresponding flight phases on the sliding mass axis is as follows:

$$\begin{aligned} W_{flight} =& (\max(0, x_{sf} - s_z(2)) \\ &+ x_{end} - s_z(2)) \cdot m_{hip} g k_{flight} \end{aligned} \tag{27}$$

Where again $k_{fleight} = 0.158$.

The cumulative work for the backwards step sequence can now be expressed from equations 16, 26, and 27 as follows:

$$W_{back} = W_{slide} + W_{sz} + W_{flight} \tag{28}$$

An inequality comparison between W_{for} and W_{back}

will determine which step sequence the sliding mass model considers less energy-intensive.

3 Results

3.1 Optimized trajectories

In trying to optimize trajectories across a wide range of initial states, the optimizer offered several basic solution patterns. In this section are images of the various trajectories, with the markers representing the hip position at evenly-spaced time intervals. The color of the markers corresponds to the phase; dark blue is the first stance phase, dark green is the second stance phase, dark red is the third stance phase, and light blue represents a flight phase. For the forwards step sequence, there is no red third stance phase since there are only two stance phases. On the ice patch the black markers represent the position of the toe at the times corresponding to the dark blue markers. The toe position at touchdown is highlighted with a bright green circle and the toe position at takeoff is highlighted with a cyan circle. The SLIP is shown at the instant of touchdown at each picture.

3.2 Sliding Mass Model Predictions

The sliding mass model correctly predicted 84.4% of the backwards step sequences, 89.0% of the forwards step sequences, and 88.0% of all step sequences. These results are summarized in Figure 3.2, and Figure 3.2 presents the sequence breakdown given by the optimizer.

4 Discussion

4.1 Sources of Error

Possible sources of error in this experiment include the following:

- Bias towards forward step sequences. 79% of optimization scenarios resulted in the forwards step sequence being more efficient (as is intuitively reasonable). Although the forwards and backwards correct percentages for the sliding mass model were comparable, the slight bias toward forward step sequences means that the overall correct percentage is slightly higher than it would have been if the scenarios had been distributed 50/50.

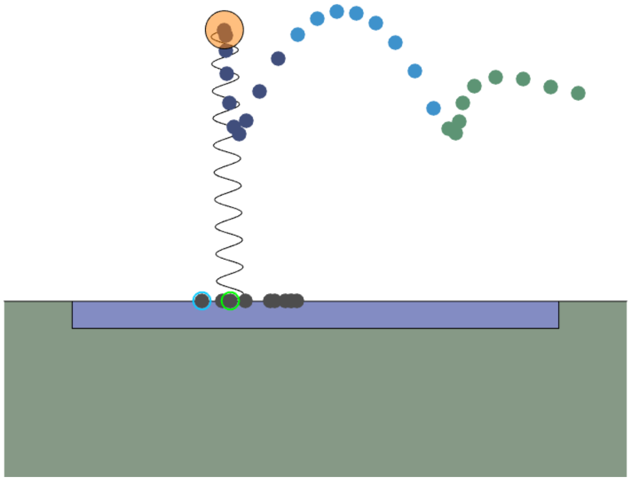

Figure 3: A 2-stance-phase forwards step simulation showing a leap. The SLIP first brings the toe forward as the hip is falling down, shown by the cluster of black markers to the right of the green ring. Then, once the spring is compressed and the normal force (hence friction force) is at a maximum, it swipes backwards rapidly (seen by the blue-ringed marker to the left). The SLIP then enters a ballistic flight phase and a short compression/decompression immediately upon landing. The leap strategy is usually energetically expensive—it might be better to first step backwards in this situation.

- Possible local optima. Although all spot-checked solutions were found to converge to the same optima from multiple initial guesses, it is still possible that some of the solutions in the dataset are missing global optima.

- A coarse discretization (10 nodes per stance phase). This relatively low node count means that physics approximations may at times break down as time durations between nodes become

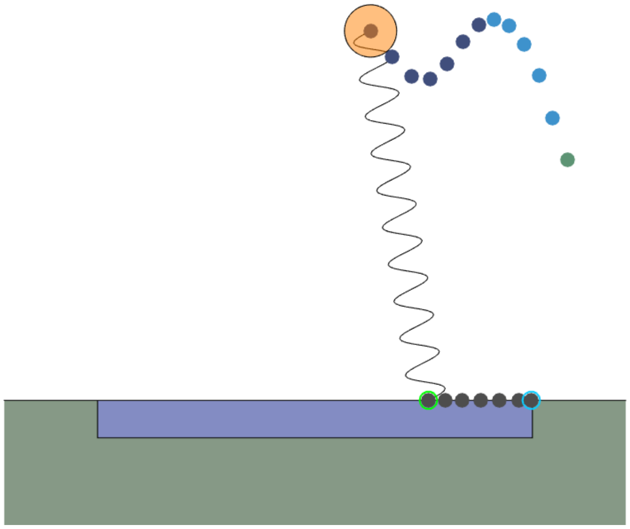

Figure 4: A 2-stance-phase forwards step simulation with a smooth slide to the end of the ice patch. As can be seen by the even spacing of the black toe markers on ice, the SLIP travels horizontally at a fairly constant velocity while undergoing spring compression. After the termination of the flight phase, the SLIP lands essentially directly at the goal position. Since there is little work done in either stance phase, the slide strategy is very energetically efficient.

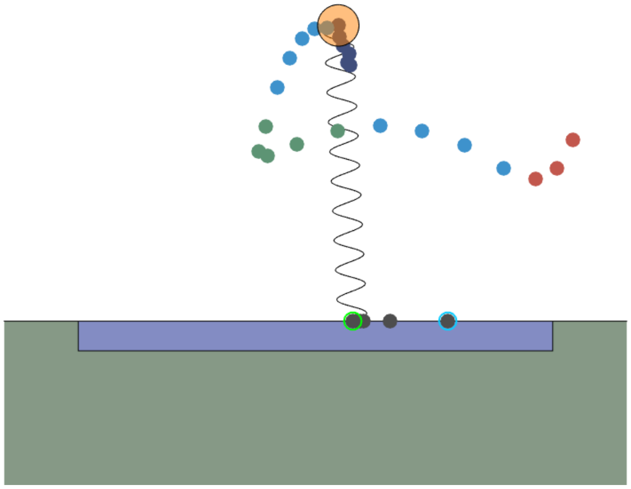

Figure 5: A 3-stance-phase backwards step simulation showing the toe swiping forwards during the first stance phase. This propels the SLIP backwards, compressing the spring and allowing it to leap over the ice patch during the second stance phase. This kind of motion is usually energy inefficient, since it involves completely reversing the direction of motion during the first stance phase and a large leap during the second.

large. This was counteracted by imposing a time limit for stance phase duration—however, this also creates the risk of forcing sub-optimal solutions in favor of faster convergence.

4.2 Analysis & Conclusion

As can be seen by the high accuracy of the sliding mass model, simple, analytically solvable models can indeed be substituted for onboard numerical trajectory optimization—which is often unfeasible due to time constraints. This could open up the possibility of real-time dynamic legged motion planning over slippery terrain. Although this study focused primarily on ice patches, similar investigations could be conducted on surfaces with more complex friction properties, such as a bed of dry leaves.

Additionally, analysis of key solutions from the optimizer indicates some promising future paths of research. Solutions fall into a few generic motion templates, whose center of mass trajectories vary slightly depending on the initial state but are similar in shape. Rough COM trajectories could potentially be generated in real time based on a template library and initial state information and then followed using some kind of a force-tracking scheme. The comparative efficiency of explicit COM tracking versus full numerical optimization could then be established as a useful benchmark for the legged control community.

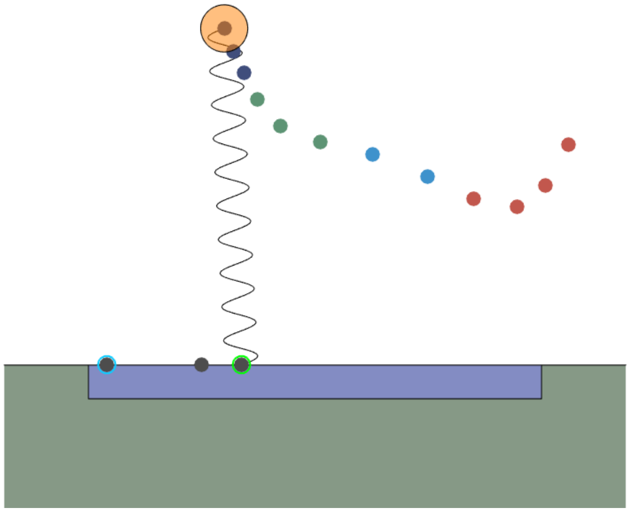

Figure 6: A 3-stance-phase backwards step simulation showing the SLIP sliding the toe backwards during the first stance phase. Unlike the previous figure, the SLIP starts close enough to the left end of the ice patch to push itself off the left side of the ground without propelling itself to the left during the first stance phase. This maneuver is usually an energy-efficient method for traversing wide ice patches.

Literature Cited

Boone, G. N. and Hodgins, J. K. (1997). Slipping and Tripping Reflexes for Bipedal Robots. *Autonomous Robots*, 1(0).

Gamus, B. and Or, Y. (2013). Analysis of dynamic bipedal robot walking with stick-slip transitions. *Proceedings - IEEE International Conference on Robotics and Automation*, pages 3348–3355.

Hubicki, C., Jones, M., Daley, M., and Hurst, J. (2015). Do Limit Cycles Matter in the Long Run? Stable Orbits and Sliding-Mass Dynamics Emerge in Task-Optimal Locomotion. *Robotics and Automation (ICRA), 2015 IEEE International Conference on*, pages 5113–5120.

Hubicki, C. M., Aguilar, J. J., Goldman, D. I., and Ames, A. D. (2016). Tractable Terrain-aware Mo-

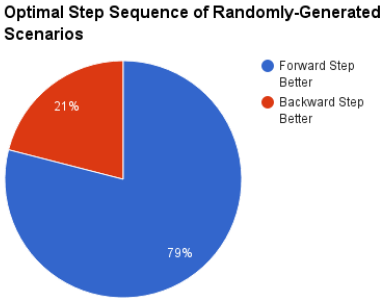

Figure 7: The breakdown of forward-step-optimal and backward-step-optimal sequences, as given by the optimizer. In 79% of the 217 simulations, the optimizer found the forward step sequence superior to the backward step sequence.

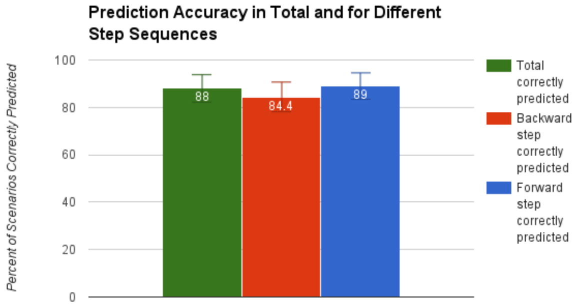

Figure 8: A bar chart comparing total correct prediction percentage and correct prediction percentages for each type of step sequence. The error bars depict the standard error. The sliding mass model was slightly better at predicting forward step sequences. However, the high overall accuracy suggests that the simplified sliding mass model can be used as an approximation of the full SLIP dynamics.

tion Planning on Granular Media: An Impulsive Jumping Study. *Intelligent Robots and Systems (IROS), 2016 IEEE/RSJ International Conference on*, pages 3887–3892.

Larson, P. and Seipel, J. (2012). A spring-loaded inverted pendulum locomotion model with radial forcing. *ASME 2012 International Design Engineering Technical Conferences and Computers and Information in Engineering Conference*, pages 877–883.

Or, Y. and Moravia, M. (2016). Analysis of Foot Slippage Effects on an Actuated Spring-mass Model of Dynamic Legged Locomotion. *International Journal of Advanced Robotic Systems*, page 1.

Piovan, G. and Byl, K. (2012). Enforced symmetry of the stance phase for the Spring-Loaded Inverted Pendulum. *Proceedings - IEEE International Conference on Robotics and Automation*, pages 1908–1914.

Poulakakis, I. and Grizzle, J. W. (2007). Formal embedding of the spring loaded inverted pendulum in an asymmetric hopper. *Proc. of the European Control Conference*, pages 1–8.

Raibert, M. H., Blankespoor, K., Nelson, G., and Playter, R. (1986). Legged robots. *Communications of the ACM*, 29(6):499–514.

Saranli, U., Arslan, O., Ankarali, M. M., and Morgul, O. (2010). Approximate analytic solutions to non-symmetric stance trajectories of the passive Spring-Loaded Inverted Pendulum with damping. *Nonlinear Dynamics*, 62(4):729–742.

Srinivasan, M. and Ruina, A. (2006). Computer optimization of a minimal biped model discovers walking and running. *Nature*, 439(7072):72–75.